PAPER

Check for updates

Size and morphology control over MOF-74 crystals†

Chunhui Wu, [ID] *[a] Xinxin Chu,[a] Xiaoling Wu, [ID] [ab] He Zhou,[a] Youshi Zeng,[a] Dongxu Wang[c] and Wei Liu[ab]

Precise control of the size and morphology of metal–organic framework (MOF) crystals is challenging yet critical for the expansion of the application potential of MOF materials. This work presents a detailed investigation of the impact of various synthetic conditions such as reactant ratio, acidity, capping agent, reaction solution (H_2O, ethanol and DMF) *etc.* on the size and morphology of Mg-MOF-74, a classical MOF with record high CO_2 uptake capacity. By varying these fabrication parameters and modulators, the morphology and size of crystals can be precisely tuned in the nanometer to micrometer range. Particularly, the nanosized flaky Mg-MOF-74 crystals with an aspect ratio of ∼0.5 were synthesized for the first time by varying the amount of water. The MOF-74 crystals with different size and morphologies are good candidates for more advanced applications favored by crystal size and morphology control.

Introduction

Metal–organic frameworks (MOFs) are a new class of porous materials formed by coordination of metal-containing secondary building units (SBUs) and organic ligands. The diversity of metal and organic ligands endows the obtained MOFs with structural versatility as well as unique physical and chemical properties, including high specific surface areas, regular shaped pore channels, controllable pore sizes and porosities, and tunable functional groups. These advantages have led to a wide range of applications of MOF in catalysis, gas storage and separation, batteries, sensing, biomedicine, and other fields.[1–10]

Current research about MOFs mainly focuses on the design, synthesis, characterization and application of bulk MOFs materials. However, some applications of MOFs depend not only on the ability to control the chemical structure of a material but also its microstructure, size, and morphology. For example, high quality MOF films or membranes require precise control of the size and orientation of the individual MOF crystals.[11–14] It is reported that the downsizing MOF particles have advantages over bulk phase MOFs in the areas of catalysis, chemical sensing and gas separation due to their short diffusion pathway and extended external surface areas, which leads to accelerated mass transport of guest molecules and more accessible catalytic active sites.[15–19] Therefore, tailoring the size and morphology of MOF crystals is of paramount importance.

MOF-74 is a series of prototypical MOFs constructed by linking divalent metal ions ($M^{2+} = Mg^{2+}$, Zn^{2+}, Ni^{2+}, Co^{2+}, Fe^{2+}, Mn^{2+}, and Cu^{2+}) with 2,5-dihydroxyterephthalic acid (DOT) linker into a 3-D crystalline network featuring 1-D hexagonal channels of ∼1.1 nm diameter (Fig. S1†).[20–23] The presence of high-density open metal sites endows MOF-74 with excellent gas adsorption properties valuable for a range of applications.[24–28] Unfortunately, the synthesis of well-defined MOF-74 colloidal particles with tunable size and aspect ratio is still challenging due to a lack of knowledge on how various synthetic parameters can impact its crystal morphology. In 2019, we reported the synthesis of uniform and well-defined Mg-MOF-74 nanocrystals with extremely low polydispersity index (PDI) of 1.02 and tunable aspect ratio through simultaneous pH regulation and modulator control.[16] We demonstrated that downsizing the pore length of MOF-74 crystal leads to a faster gas adsorption and separation kinetics.

Following in the footsteps of the previous work, the influence of Mg-MOF-74 synthetic parameters such as the reactant ratio, reaction solution, acidity, concentration and type of capping agent was studied in-depth in this work (Scheme 1). The aim is to understand the principle of size and morphology control over MOF-74 crystals. Based on the principle, the size and morphology of MOF-74 crystals can be precisely regulated at nanoscale and microscale. It is worth noting that the nanosized flaky Mg-MOF-74 crystals with an aspect ratio of ∼0.5 were synthesized by size and morphology control, which was the first reported to date.

[a]Shanghai Institute of Applied Physics, Chinese Academy of Sciences, Shanghai, China 201800. E-mail: wuchunhui@sinap.ac.cn

[b]Wuwei Institute of Advanced Energy, Gansu Province, China 733099

[c]School of Physical Science and Technology, ShanghaiTech University, Shanghai 201210, People's Republic of China
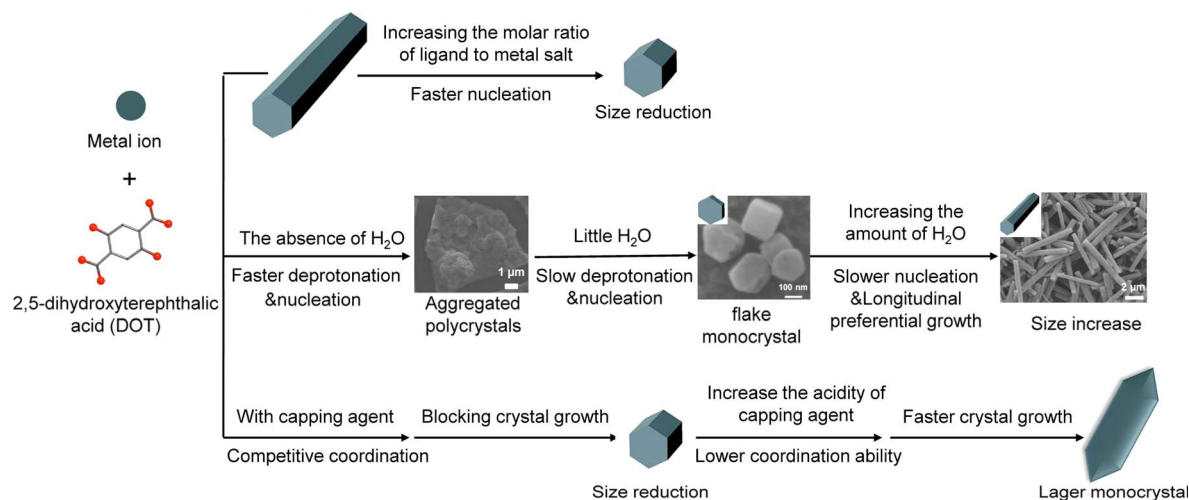
Scheme 1 Schematic illustration of the mechanism for size and morphology controllable synthesis of MOF-74 crystals.
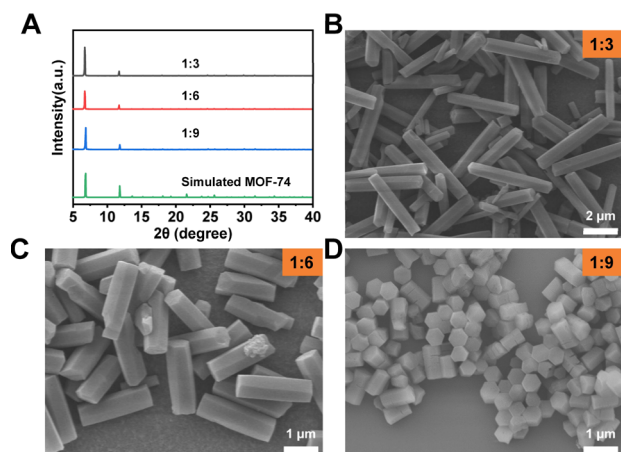

Fig. 1 (A) PXRD patterns of Mg-MOF-74 synthesized with various molar ratios of ligand and metal salt. (B–D) SEM images of Mg-MOF-74 synthesized with various molar ratio of ligand and metal salt.

Results and discussions

Through the pH and acetic acid (HOAc) modulator control, our previous work has established that when the molar ratio between DOT and $Mg(NO_3)_2 \cdot 6H_2O$ is 1 : 9 with 5 equiv. (with respect to DOT) HOAc and a pH value of 9.55, uniform and well-defined Mg-MOF-74 nanocrystals can be synthesized through microwave assisted synthesis (Fig. 1D).[16] Based on this knowledge, we further investigated the effect of other synthesis parameters on the size and morphology of Mg-MOF-74. Firstly, we studied the influence of the molar ratio of ligand and metal salt on the crystallization of Mg-MOF-74. By maintaining the pH value at 9.55 ± 0.05 and HOAc at 5 equiv., the molar ratio of ligand and metal salt varied from 1 : 3 to 1 : 9. The powder X-ray diffraction (PXRD) patterns and scanning electron microscopy (SEM) images show that all the reaction conditions produced Mg-MOF-74 particles with good size uniformity and crystallinity (Fig. 1). With the increase of the molar ratio between the ligand

and metal salt, the size uniformity slightly increased, but the width of the crystals decreased from ~715 nm to ~493 nm. In contrast, the length of particles drastically dropped from ~4.3 μm to ~807 nm (Fig. 1B–D). This is because a high metal salt concentration speeds up the nucleation kinetics of Mg-MOF-74, which results in the formation of a large number of nuclei at the early stage of the reaction. This has led to smaller Mg-MOF-74 crystals with a homogeneous size distribution (Scheme 1).[29]

Furthermore, the influence of crystal size and morphology on the pore structure was studied. The Mg-MOF-74 (1 : 3) has similar N_2 adsorption isotherm at 77 K and BET surface area (1217 cm^3 g^{-1}) compared to that of Mg-MOF-74 (1 : 9) (1211 cm^3 g^{-1}) (Fig. S2a†), and the pore-size distribution analysis showed Mg-MOF-74 (1 : 3) and Mg-MOF-74 (1 : 9) has consistent pore size centering (1.13 nm) (Fig. S2b†), which demonstrates that the crystallinity and porosity of Mg-MOF-74 was not affected by the crystal size and morphology.

Next, we investigated the effect of the reaction solution on the size and morphology of Mg-MOF-74 crystals. The reaction solution is a 1 : 1 : 1 (v/v/v) mixture of water, *N,N*-dimethylformamide (DMF) and ethanol. In order to explore the influence of H_2O, the amount of water was varied from 0 to 13 mL while other synthesis parameters remained unchanged relative to previous synthetic condition.[16] As shown in Fig. S3a,† polycrystalline Mg-MOF-74 aggregates were obtained in the absence of H_2O. The broad PXRD peak indicates that these aggregates consist of nanocrystals of Mg-MOF-74 (Fig. S4†). With the addition of 1 mL H_2O, the morphology of the aspherical aggregate was observed. These aggregates were joined by ~20 nm Mg-MOF-74 crystallites (Fig. S3b†). Continuously increasing the amount of H_2O to 3–13 mL, monodispersed Mg-MOF-74 single crystals were formed (Fig. 2). Fusiform-shaped crystals were obtained when 13 mL water was added to the reaction, whereas crystals with a classic hexagonal pillar shape tend to dominate otherwise (3–9.5 mL H_2O). Interestingly, with an increasing H_2O amount, the length of crystals increases significantly from ~283 nm (3 mL H_2O) to
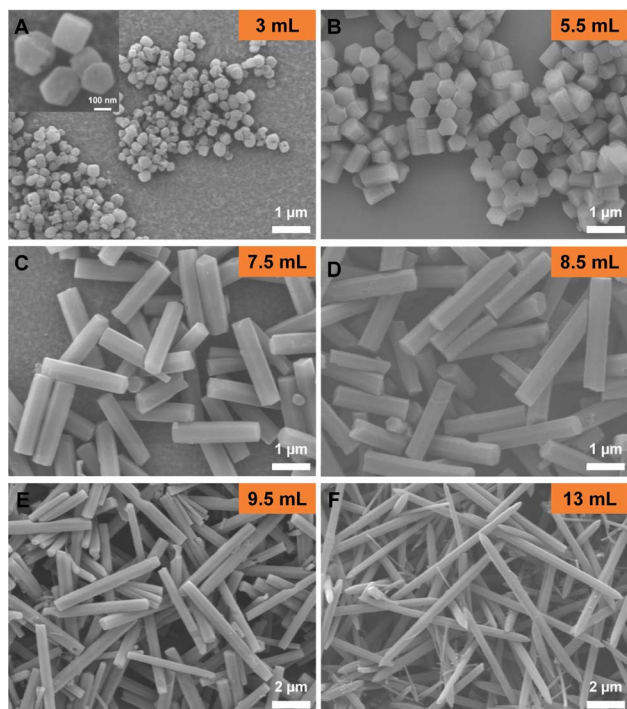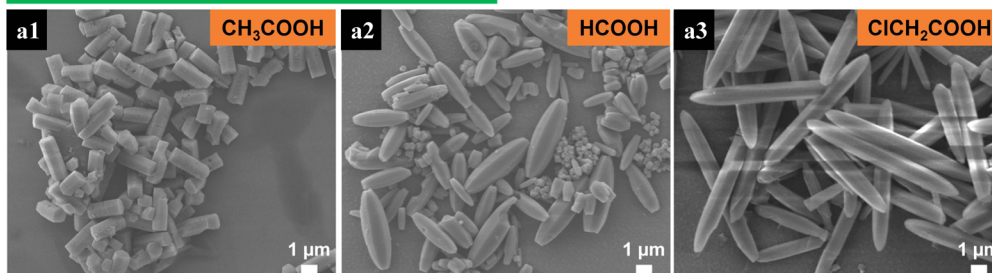
Fig. 2 (A–F) SEM images of Mg-MOF-74 synthesized with various amounts of water.

~9.3 μm (13 mL H_2O). Meanwhile, the width of the crystals only slightly increased from ~251 to ~507 nm (Fig. 2). This is likely because water has an influence on the deprotonation of DOT. In the absence of water, the deprotonation of DOT was fast and

produced a crystal aggregate. As water was introduced into the solution as a mixed solvent, it inhibited the deprotonation of DOT and reduced its solubility in the reaction mixtures, resulting in a decreased amount of deprotonated DOT ions available for coordination and slowed nucleation rates, which led to increased crystal size (Scheme 1).[30] Meanwhile, water promoted crystal growth in the longitudinal growth direction, which led to the longitudinal growth rate is much faster than the lateral. On the other hand, the particle size of the crystal aggregate was reduced due to the dispersive action of water. As a result, the size and morphology of MOF-74 crystals can be precisely regulated at the nanoscale to microscale through controlling the amount of water. In particular, when the amount of water was 3 mL, nanosized flaky Mg-MOF-74 crystals with an aspect ratio of ~0.5 were obtained (Fig. 2A). To the best of our knowledge, this is the first synthesis of nanosized flaky Mg-MOF-74 crystals to date. The flaky Mg-MOF-74 obtained by downsizing the longitudinal size of the crystals can greatly shorten the gas diffusion length and thus enhance its adsorption kinetics and gas separation efficiency, which is much more efficient and simpler compared to our previously reported method of shortening the diffusion length by preparing hollow MOF-74.[16]

Furthermore, the influence of DMF and ethanol was also studied. As shown in Fig. S5,† the absence of DMF or ethanol led to the formation of large and polydisperse products. This is likely because the decreasing ligand solubility caused by the absence of DMF or ethanol inhibits the nucleation process which results in the formation of large crystals with an inhomogeneous size distribution.
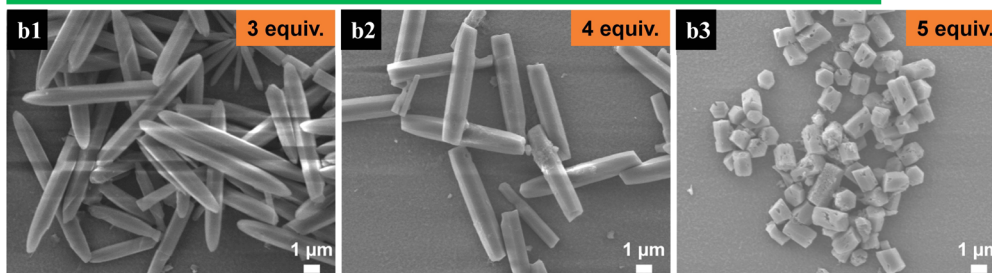

Fig. 3 (A) SEM images of Mg-MOF-74 synthesized with capping agents of various acidity. (B) SEM images of Mg-MOF-74 synthesized with different amounts of chloroacetic acid.
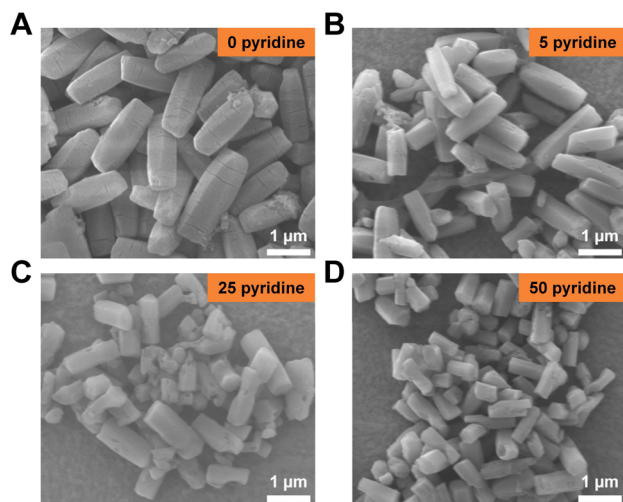
Fig. 4 (A–D) SEM images of Mg-MOF-74 synthesized with various amount of pyridine.

In our previous synthetic condition for Mg-MOF-74 (5 equiv. HOAc, pH = 9.55), HOAc serves as a capping agent which can coordinate with the metal ions to compete with the DOT at high pH value. Thus, the longitudinal growth rate of the crystallites was effectively reduced. In the present study, in order to deeply study the effect of capping agent acidity on Mg-MOF-74 crystal size and morphology, 3 equiv. HOAc, carboxylic acid (HCOOH) and chloroacetic acid (ClCH$_2$COOH) were added respectively as capping agents while the pH was maintained at 9.55 ± 0.05. The order of acidity is ClCH$_2$COOH (pK_a = 2.86, 25 °C) > HCOOH (pK_a = 3.75, 25 °C) > CH$_3$COOH (pK_a = 4.76, 25 °C) in water solution. It is worth noting that fusiform-shaped crystals were obtained for ClCH$_2$COOH and HCOOH whereas hexagonal rods were obtained for CH$_3$COOH (Fig. 3A and S6†). With increasing acidity, the width of the crystals slightly increased from ~0.99 μm (CH$_3$COOH) to ~1.1 μm (ClCH$_2$COOH). In contrast, the length of particles drastically raised from ~2.5 μm to 10.1 μm. This is because a stronger acid has a weaker conjugate based and thus coordination ability (i.e., ClCH$_2$COO$^-$ < HCOO$^-$ < CH$_3$COO$^-$ in terms of basicity). As a result, a stronger coordinating capping agent has a greater capability to inhibit the longitudinal growth of the Mg-MOF-74 crystallites (Scheme 1).[31]

Similar to the HOAc capping agent, the influence of chloroacetic acid concentration on the morphology and size of Mg-MOF-74 was also investigated. As expected, with the increase of chloroacetic acid, the length of crystals decreases significantly from ~10.1 μm (3 equiv.) to ~1.5 μm (5 equiv.) while the width remained the same (~1.2 μm) (Fig. 3B and S7†). This result is consistent with that of acetic acid as a modulator.[16]

Besides carboxylic acids, organic bases or even inorganic modulators can also exert analogous effects. For instance, Cho et al. synthesized rod-, lump-, and disk-shaped porous coordination polymers in the presence of pyridine as the capping agent.[32] Thus, we turned to studying the effect of pyridine on Mg-MOF-74 morphology. By maintaining the pH at 9.55 ± 0.05, the amount of pyridine was varied from 0 to 50 equiv. (with

respect to DOT). All the obtained PXRD patterns correspond to the Mg-MOF-74 structure (Fig. S8†). It is worth noting that fusiform-shaped crystals were obtained in the absence of pyridine whereas hexagonal rods tend to dominate otherwise (Fig. 4). With the amount of pyridine increasing from 0 to 50 equiv., the width of the crystals decreased from ~672 nm to ~382 nm, and the length of particles dropped from ~1.8 μm to ~770 nm (Fig. 4). The decrease in the size of Mg-MOF-74 crystals is caused by the presence of pyridine which serves as a capping agent to block further crystal growth (Scheme 1).

Conclusions

In summary, the effects of the reactant ratio, reaction solution, acidity, amount and type of capping agent on the size and morphology of the Mg-MOF-74 products have been independently investigated. With the increase of the molar ratio of ligand and metal salt, the size uniformity slightly increased, and the length drastically decreased due to the fast crystal nucleation kinetics. With the decrease of the water amount, Mg-MOF-74 crystals with decreased aspect ratio can be obtained. As a result, the size and morphology of Mg-MOF-74 crystals can be precisely regulated at the nanoscale to microscale through controlling the amount of water. Particularly, the nanosized flaky Mg-MOF-74 crystals with an aspect ratio of ~0.5 were obtained by optimizing the amount of water. Regarding the influence of the capping agent, we found that the size of crystals increases significantly with increasing acidity of the capping agent due to weaker coordination ability. In addition, as the amount of capping agent increases, the longitudinal growth rate of Mg-MOF-74 was inhibited, which leads to a significant decrease in crystal length. This work is instructive for the size and morphology control of MOFs and, more importantly, is crucial in the MOFs applications favored by crystal size and morphology control.

Data availability

The authors confirm that the data supporting the findings of this study are available within the article and its ESI.†

Conflicts of interest

There are no conflicts to declare.

Acknowledgements

Notes and references

1 H. Furukawa, K. E. Cordova, M. O'Keeffe and O. M. Yaghi, *Science*, 2013, **341**, 1230444.

2 S. Kitagawa, *Chem. Soc. Rev.*, 2014, **43**, 5415–5418.

3 O. K. Farha and J. T. Hupp, *Acc. Chem. Res.*, 2010, **43**, 1166–1175.

4 K. Sumida, D. L. Rogow, J. A. Mason, T. M. McDonald, E. D. Bloch, Z. R. Herm, T.-H. Bae and J. R. Long, *Chem. Rev.*, 2011, **112**, 724–781.

5 G. Maurin, C. Serre, A. Cooper and G. Férey, *Chem. Soc. Rev.*, 2017, **46**, 3104–3107.

6 B. Li, H.-M. Wen, W. Zhou, J. Q. Xu and B. Chen, *Chem*, 2016, **1**, 557–580.

7 J. A. Mason, M. Veenstra and J. R. Long, *Chem. Sci.*, 2014, **5**, 32–51.

8 R. B. Getman, Y.-S. Bae, C. E. Wilmer and R. Q. Snurr, *Chem. Rev.*, 2012, **112**, 703–723.

9 C. P. Raptopoulou, *Materials*, 2021, **14**, 310.

10 J. Yang and Y. W. Yang, *Small*, 2020, **16**, 1906846.

11 O. Shekhah, J. Liu, R. Fischer and C. Wöll, *Chem. Soc. Rev.*, 2011, **40**, 1081–1106.

12 D. Zacher, O. Shekhah, C. Wöll and R. A. Fischer, *Chem. Soc. Rev.*, 2009, **38**, 1418–1429.

13 Y. Cheng, S. J. Datta, S. Zhou, J. Jia, O. Shekhah and M. Eddaoudi, *Chem. Soc. Rev.*, 2022, **51**, 8300–8350.

14 C. R. Marshall, S. A. Staudhammer and C. K. Brozek, *Chem. Sci.*, 2019, **10**, 9396–9408.

15 H. Uehara, S. Diring, S. Furukawa, Z. Kalay, M. Tsotsalas, M. Nakahama, K. Hirai, M. Kondo, O. Sakata and S. Kitagawa, *J. Am. Chem. Soc.*, 2011, **133**, 11932–11935.

16 C. Wu, L.-Y. Chou, L. Long, X. Si, W.-S. Lo, C.-K. Tsung and T. Li, *ACS Appl. Mater. Interfaces*, 2019, **11**, 35820–35826.

17 K. H. Park, K. Jang, S. U. Son and D. A. Sweigart, *J. Am. Chem. Soc.*, 2006, **128**, 8740–8741.

18 J. Wang, I. Imaz and D. Maspoch, *Small Struct.*, 2022, **3**, 2100126.

19 A. L. Semrau, P. M. Stanley, A. Urstoeger, M. Schuster, M. Cokoja and R. A. Fischer, *ACS Catal.*, 2020, **10**, 3203–3211.

20 N. L. Rosi, J. Kim, M. Eddaoudi, B. Chen, M. O'Keeffe and O. M. Yaghi, *J. Am. Chem. Soc.*, 2005, **127**, 1504–1518.

21 Q. Zhang, B. Li and L. Chen, *Inorg. Chem.*, 2013, **52**, 9356–9362.

22 M. J. Katz, A. J. Howarth, P. Z. Moghadam, J. B. DeCoste, R. Q. Snurr, J. T. Hupp and O. K. Farha, *Dalton Trans.*, 2016, **45**, 4150–4153.

23 T. Xiao and D. Liu, *Microporous Mesoporous Mater.*, 2019, **283**, 88–103.

24 R. Krishna and J. R. Long, *J. Phys. Chem. C*, 2011, **115**, 12941–12950.

25 E. D. Bloch, W. L. Queen, R. Krishna, J. M. Zadrozny, C. M. Brown and J. R. Long, *science*, 2012, **335**, 1606–1610.

26 L. C. Lin, J. Kim, X. Kong, E. Scott, T. M. McDonald, J. R. Long, J. A. Reimer and B. Smit, *Angew. Chem., Int. Ed.*, 2013, **52**, 4410–4413.

27 D.-L. Chen, H. Shang, W. Zhu and R. Krishna, *Chem. Eng. Sci.*, 2015, **124**, 109–117.

28 J. H. Choe, H. Kim and C. S. Hong, *Mater. Chem. Front.*, 2021, **5**, 5172–5185.

29 Y. Han, M. Liu, K. Li, Y. Zuo, Y. Wei, S. Xu, G. Zhang, C. Song, Z. Zhang and X. Guo, *CrystEngComm*, 2015, **17**, 6434–6440.

30 X. Cheng, A. Zhang, K. Hou, M. Liu, Y. Wang, C. Song, G. Zhang and X. Guo, *Dalton Trans.*, 2013, **42**, 13698–13705.

31 D. Jiang, C. Huang, J. Zhu, P. Wang, Z. Liu and D. Fang, *Coord. Chem. Rev.*, 2021, **444**, 214064.

32 W. Cho, H. J. Lee and M. Oh, *J. Am. Chem. Soc.*, 2008, **130**, 16943–16946.